




Article

The 21st August 2020 Flood in Douala (Cameroon): A Major Urban Flood Investigated with 2D HEC-RAS Modeling

Junior Yves-Audrey Iroume ^{1,2,3,*} , Raphaël Onguéné ^{1,3}, Francis Djanna Koffi ¹, Antoine Colmet-Daage ⁴, Thomas Stieglitz ⁵ , Willy Essoh Sone ⁶, Sakaros Bogning ^{2,3} , Joseph Magloire Olinga Olinga ⁷, Romaric Ntchantcho ², Jean-Claude Ntonga ², Jean-Jacques Braun ^{3,8}, Jean-Pierre Briquet ⁹ and Jacques Etame ¹

- ¹ Technology and Applied Science Laboratory, University Institute of Technology, University of Douala, Douala P.O. Box 8698, Cameroon; ziongra@yahoo.fr (R.O.); djannaj@gmail.com (F.D.K.); etame.jacques@yahoo.fr (J.E.)
- ² Institute of Geological and Mining Research, Vogt Street, Yaoundé P.O. Box 4110, Cameroon; sakarosb@gmail.com (S.B.); ntchantcho@yahoo.fr (R.N.); ntonga_jc@yahoo.fr (J.-C.N.)
- ³ Laboratoire Mixte International—Dynamique des Ecosystèmes Continentaux d’Afrique Centrale (LMI-DYCOFAC), Institut de Recherche pour le Développement, Yaoundé P.O. Box 1857, Cameroon; jbraun1@gmail.com
- ⁴ Philia Ingenierie, 193 Avenue Jean Rieux, 31500 Toulouse, France; antoine.colmet-daage@philia-ingenierie.fr
- ⁵ Aix-Marseille Université, CNRS, IRD, INRAE, Coll France, CEREGE, 13100 Aix-en-Provence, France; stieglitz@cerege.fr
- ⁶ Ecosystems and Fishery Resources Laboratory, Institute of Fisheries and Aquatic Sciences, University of Douala, Douala P.O. Box 2701, Cameroon; pharellwilly2@yahoo.fr
- ⁷ Douala Urban Council (DUC), Douala P.O. Box 1857, Cameroon; joseph_olinga87@yahoo.fr
- ⁸ Géosciences et Environnement, Toulouse (Université de Toulouse, CNRS, IRD), 14 Avenue Edouard Berlin, 31400 Toulouse, France
- ⁹ HydroSciences Montpellier, Université de Montpellier, CNRS, IRD, 300 Av. Pr E. Jeanbrau, 34090 Montpellier, France; jean-pierre.bricquet@ird.fr
- * Correspondence: iroumejunior21@outlook.fr; Tel.: +237-695-71-71-98



Citation: Iroume, J.Y.-A.; Onguéné, R.; Djanna Koffi, F.; Colmet-Daage, A.; Stieglitz, T.; Essoh Sone, W.; Bogning, S.; Olinga Olinga, J.M.; Ntchantcho, R.; Ntonga, J.-C.; et al. The 21st August 2020 Flood in Douala (Cameroon): A Major Urban Flood Investigated with 2D HEC-RAS Modeling. *Water* **2022**, *14*, 1768. <https://doi.org/10.3390/w14111768>

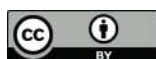
Academic Editor: Renato Morbidelli

Received: 13 April 2022

Accepted: 20 May 2022

Published: 31 May 2022

Publisher’s Note: MDPI stays neutral with regard to jurisdictional claims in published maps and institutional affiliations.



Copyright: © 2022 by the authors. Licensee MDPI, Basel, Switzerland. This article is an open access article distributed under the terms and conditions of the Creative Commons Attribution (CC BY) license (<https://creativecommons.org/licenses/by/4.0/>).

Abstract: A major flood event occurred on 21 August 2020 in the densely populated Makèpè Missokè neighborhood in the city of Douala (Cameroon, Africa). Nearly 2210 buildings and 12,376 victims spread over 82 hectares were affected. A 2D HEC-RAS model is applied to simulate and characterize this event. A cross analysis of flood depth and flow velocity is used to classify the flood risk and identify areas exposed from low to high hazard. The simulations provide detailed information on the flood characteristics (extent, depth, velocity, arrival time, and duration). The simulated maximum water surface profiles are consistent with the floods marks with differences ranging from 0.02 m to 0.44 m, indicating a good agreement between the observed and simulated water levels at the peak flow ($NSE = 0.94$, $Erel = 0.92$, $RMSE = 0.21$ m). The maximum inundation level is 4.48 m and the flow velocity is globally low at less than 1 m/s. The average flood arrival time and duration are 5 h and 26 h, respectively, for a threshold height of 0.5 m. These results indicate a fast mobilization of the major river channel for the evacuation of this flood. The level of accuracy of the developed model of the 21 August 2020 flood event is appropriate for flood hazard assessment in the city of Douala and is designed to find operational application in future events.

Keywords: flood hazard assessment; HEC-RAS; hydraulic modeling; Tongo Bassa watershed; urban floods

1. Introduction

Many studies suggest that climate change may result in more frequent and intense floods hazards [1–3]. Tropical fast-growing cities in developing countries are expected to be the most affected [4–7]. The city of Douala in Cameroon (Central Africa) is a coastal megacity (with more than 4 million inhabitants) that is regularly affected by floods [8–19]. An increase in the frequency and magnitude of flooding in the city has been observed

between 1980 and 2018 [19], despite a decrease in overall rainfall [15,20]. The floods' impact is exacerbated by insufficient and inadequate urban planning strategies, which favor urban sprawl [12,21–24]. The consequences are disastrous: more than 100 deaths between 2000 and 2010 [17,18,25], significant material damages [17], and economic losses not yet evaluated. Moreover, the absence of flood risk memory and conservation of flood markers [26,27] means that flooded areas are rebuilt in the aftermath of disasters, remaining vulnerable to future events [28]. In addition, floods often occur at night or early in the morning due to the high frequency of intense nightly rainfall, sometimes surprising the inhabitants in their beds [29]. This situation increases the vulnerability to floods of the residents and limits the deployment of emergency services.

The authorities' strategies to respond to these flooding events in the city of Douala are reactive than proactive [10–12,15,22,25,30–33]. They are generally based on ad hoc operations improvised in the aftermath of disasters without prior operational planning. More recently, attempts have been made to reduce flood consequences by rehabilitating gutters, cleaning main drains, and restoring the watercourses in their major bed by clearing and demolishing the constructions that are built there prior to periods of expected flood events [31]. These management strategies have shown limited results when comparing the financial resources deployed and the observed flood reduction [22,30–33]. Today, Cameroon's adherence to the Hyogo (2005–2015) and Sendai (2015–2030) frameworks for disaster risk reduction has given a new perspective to flood management in the country based on planned adaptation actions [30,34]. This orientation has resulted in the elaboration of national guidelines for identifying, characterizing, and mapping zones exposed to natural hazards and the proposed associated mitigation measures [18]. Several studies have been undertaken to understand floods in the study area [5,9,12–15,19,25,29,31,35–40]. According to them, sea level rise, extreme rainfall, and storm events often attributed to climate change have been suggested to exacerbate floods in the coastal city of Douala. Monitoring of a specific area has been implemented to provide scientific answers to this evolution and eventually to propose strategies to mitigate the consequences associated with flooding. In this context, the deployment of observation devices and measurements coupled with modeling and simulation are expected to play a key role.

Hydraulic modeling is nowadays one of the most widely used tools for flood hazard mapping [3]. Several hydraulic modeling tools (e.g., FLO-2D, SRH-2D, IBER, LISFLOOD-FP, HEC-RAS, FLORA-2D, TUFLOW, MIKE FLOOD, XP-SWMM, River-Flow2D, Telemac) are used in various studies for flood analyses [41–49]. Recent developments (1D, 2D, 1D/2D coupling) of the Hydrologic Engineering Center River Analysis System (HEC-RAS 6.0), an application developed by the U.S. Army Corps of Engineers Hydrologic Engineering Centre (USACE HEC, Davis, CA, USA), have allowed the analysis of a variety of problems, including mapping and prediction of flood-prone areas [50–58], modeling of past floods [55,59,60], extrapolation of rating curves [61], discharges estimation [61–64], simulation of dam or levee failure [65–67], impact of different development scenarios [68,69], and sediment transport [70,71].

To date, no study has been devoted to the analysis of the Douala city's flood events using state-of-the-art hydraulic modeling. This study attempted to apply a comprehensive methodology for analyzing flood risk induced by the extreme flood event that took place in the Makèpè Missokè neighborhood in August 2020. The 2D HEC-RAS model was used to delineate the flood extent for that day and provide flood components (water depth and velocity, arrival time and duration, hazard classification).

2. Study Area

The city of Douala is the economic capital of Cameroon (Figure 1A), located at the Wouri river estuary (Figure 1B). The climate is characterized by abundant rainfall almost every year with an annual average of about 4000 mm [12,15,19,20]. Rainfall is distributed around two main periods, a wet season (March to November) characterized by abundant rainfall and a dry season (December to February) [35].

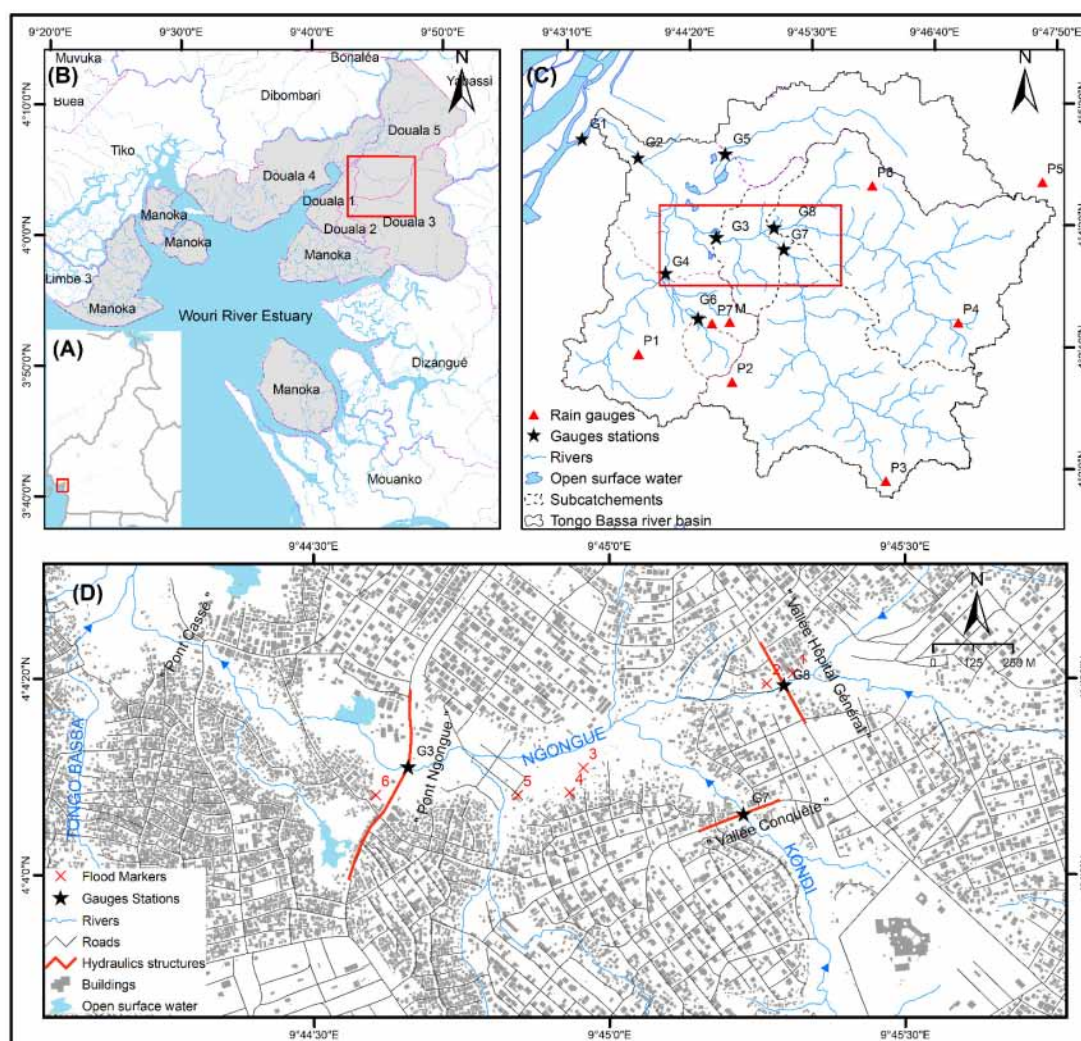


Figure 1. (A) Location of the city of Douala on the Cameroon map. (B) Wouri river estuary, tributaries, and surrounding districts. Douala subdivisions are presented in grey. (C) Location of the Makèpè Missokè district in the Tongo Bassa catchment area and presentation of the environmental observatory. The rain gauge stations (P1 to P7) are labeled by red triangles, the water level gauge stations (G1 to G8) are labeled by circles of the same color as the sub-basin limits drained, and the weather station is labeled as M. (D) Presentation of the Makèpè Missokè area, the hydrographic network, built-up areas, roads, hydraulics structures, and flood markers associated with the 21st August 2020 flood event.

Makèpè Missokè is a central and popular neighborhood of the metropolis (Figure 1D). This district is drained by the Ngongue River, the main watercourse of the Tongo Bassa watershed (Figure 1C). This basin of 42 km² located between longitude 9°46" N and latitude 4°4" N is the largest in the city and covers nearly 27 districts. The population density ranges from 25 to more than 380 inhabitants per hectare with an average household size between 5 and 6 people [34,72]. The altitudes in the catchment are less than 60 m above sea level and the average slope is about 6%. The drainage network in the Tongo Bassa watershed is dendritic with a drainage density of about 2 km/km² [72]. Four main rivers drain this catchment, named Ngongue, Tongo-Bassa, Kondi, and Moussadi (Figure 1C). The rivers' outlets into the Wouri River estuary predispose them to the tidal influence received from the Atlantic Ocean, which result in a reversal of the water flow direction at high tide [14,40,73]. Much of the catchment is urbanized, with sparse shrubs and herbaceous plants maintained in the garden and agricultural areas located along the watercourses [12,13,35,36,74]. The intertidal zone near the outlet is dominated by a mangrove that plays a protective role against coastal flooding [12,73,74].

The Douala Urban Council (DUC) has installed an environmental observatory (see Figure 1C) in the Tongo Bassa watershed within the framework of the “Douala, Sustainable City project”. This observatory is made up of 16 stations including 7 rain gauges located at the head of the watershed, 8 water level gauges throughout the catchment, and 1 weather station. The equipment's installed were designed and manufactured by OTT Hydromet (see <https://www.otthydromet.com/en/>, accessed on 12 July 2021 for more information), a company based in Kempten, Germany and Loveland, CO, USA specialized in telemetry. The rain gauges' stations (P1–P7 and M) consist of a Lambrecht 15189 precipitation sensor connected to an OTT data logger NetDL 500. The gauging stations (G1–G8) are composed of a radar sensor OTT RLS (G1), a pressure level sensor with conductivity measurement PLS-C (G2) and a water level logger OTT ecolog 800 (G3–G8). Each water level station is equipped with an OTT staff level gauge. Two power sources are provided for water level stations, solar panel (G1 and G2) and lithium battery power (G3–G8). The G1 and G2 stations are equipped with OTT data logger NetDL 500 for data storage. The acquisition frequency varies from 5 min for rainfall measurement to 15 min for water levels. Installed between July 2018 and January 2019, this observatory provides detailed information on the hydrological behavior of the watershed.

Located in the central part of the Tongo Bassa catchment, Makèpè Missokè is the most affected neighborhood by floods reported by the national daily Cameroon Tribune in the city of Douala between 1980 and 2018 [19]. Poor road conditions hinder household waste removal and increase illegal dumping (Figure 1D). This district is therefore very often the starting point of cholera epidemics with an upsurge in malaria cases [75–79]. The study area extends upstream to the “Vallée Hôpital Général” and the “Vallée La Conquête”, and downstream to the “Pont Cassé” for a distance of about 3.5 km (see Figure 1D). Two tributaries join in this sector, the Ngongue river that drains a catchment area of 11 km² at “Vallée Hôpital Général” (G8) and the Kondi river that drains a catchment area of 10.8 km² at “Vallée La Conquête” (G7).

3. Data Acquisition

Natural processes as well as human activities have a significant impact on the flow dynamics on river basins and the modification of the spatial and temporal characteristics of the surface runoff. The topographic profile of the surface subjected to heavy rainfall is the forcing in the dynamics of water flows. Precise knowledge of this surface is a prerequisite that underlies the quality of the results that can be obtained from different types of flow modeling. Therefore, the first data acquisition and modelling effort is the one dedicated to the precise acquisition of topographic data.

3.1. Topographic Data

Adequate data for model development and calibration to support decision-making processes in flood risk management are often insufficient or unavailable. A potential opportunity is offered by open-source global remote sensing data. However, these data have commonly not had the level of detail required as model input, in particular, in complex urban topographic settings.

The Shuttle Radar Topography Mission (SRTM) data provided by National Aeronautics and Space Administration (NASA) are available at an almost global scale. In a small urban catchment, the SRTM offers coarse ground resolution that does not allow a precise characterization of urban features [80]. More importantly, the banks and the main channel of the watercourse are poorly defined in the Digital Terrain Model (DTM) obtained from the SRTM [81–83]. Assuming the SRTM as the solely available DEM for the study area, two local datasets were therefore used to improve it. The first is obtained from the Cameroonian Ministry of State Property, Surveys and Land Tenure (MINDCAF) data from 2007. It is a cloud of 40,000 ground points projected in UTM32M, with the EGM 2008 geoid as reference for the elevations. The second dataset is obtained from in situ topographic surveys carried out in March 2021 in areas where the two previous datasets showed weaknesses. It is a cloud

of 831 additional ground points strategically surveyed with a Differential Global Positioning System (DGPS) that includes embankments, banks stations, roads, and bridges. The DGPS used herein is the EMLID REACH RS 2 model (see <https://www.apglos.eu/gnss/emlid/>, accessed on 12 July 2021 for more information). This device is design by EMLID which is a company based in Hong Kong, China specialize in the manufacturing of low cost Real Time Kinematic Global Navigation Satellite System (RTK GNSS) receiver.

These datasets are merged and interpolated using the 3D polylines option included in the topographic tool RD 12 version 6.12, to obtain a more precise DTM of the study area. In the study area, we now have a DTM where the flood plain, the main channel, the banks, and the hydraulics constraints due to embankments, bridges, and roads are clearly defined. However, it is important to mention that the preprocessing aims to clearly define the main channel that is less represented by the SRTM DTM. Some uncertainties associated with the representation of the floodplain require further exploration and can be achieved with a Lidar-based DTM not currently available.

3.2. Hydrological and Hydraulic Data

The most important rainfall event recorded in the Tongo Bassa watershed since data acquisition started is the 21st August 2020 event. According to the affected residents, it is the most significant event over the past 20 years. The cumulative rainfall over the catchment area varied between 194 mm and 288 mm this day. Note that operating anomalies were observed at some water level gauge stations (G1, G4, and G5), which were, therefore, unable to record this flood.

The hydrographs obtained from [64] were used as boundary conditions in the 2D HEC-RAS model upstream from the bridges located at “Vallée La Conquête” and “Vallée Hopita Général (Figure 2). HEC-DSSVue version 3.2.3 is a visual utilities program that allows one to plot, tabulate, edit, and manipulate scientific data in the HEC-DSS (Hydrologic Engineering Center Data Storage system) database file. The choice of this tool is justified by its flexibility of use and the possibility of direct interfacing with HEC-RAS in reading and writing.

A campaign to measure and characterize high water marks was carried out in 22 August 2020 after the flood event (Figure 1D). In the areas where we have doubts on water marks, a household survey allowed us to retrieve information on the highest water levels reached in the study area. The highest water levels obtained during this investigation were levelled during the topographic survey in March 2021. These data were used for model calibration on the 21 August 2020 flood event.

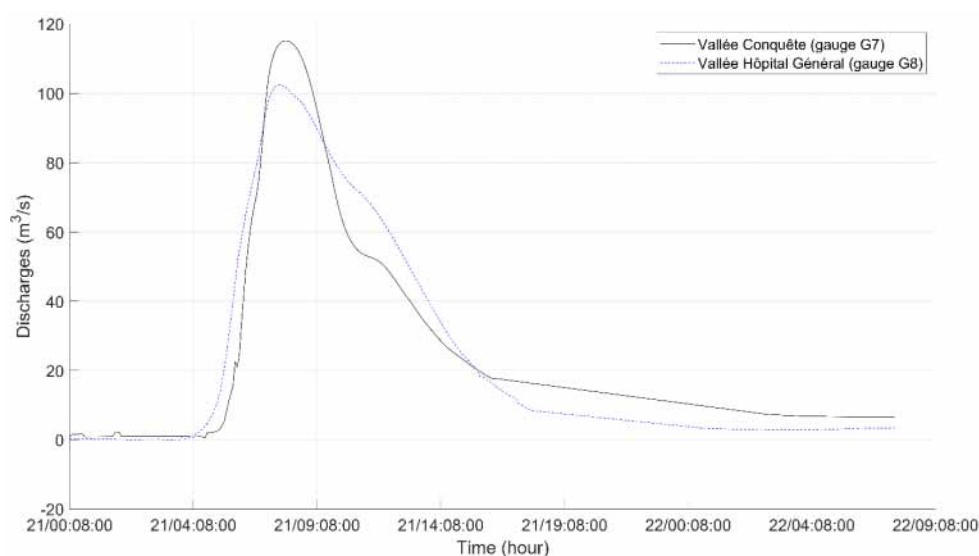


Figure 2. Hydrographs at “Vallée La Conquête” and “Vallée Hôpital Général” used as boundary conditions in the 2D HEC-RAS model.

3.3. Land-Use and Built-Up Data

The built-up areas were obtained from the openstreetmap database (2020 version) for the city of Douala (Figure 1D). The land use data were deduced by manually on-screen digitizing polygons from Google Earth. Two main classes were identified, i.e., the built-up areas and the natural vegetation. The values of Manning's coefficients were defined according to standard values based on United States Geological Survey (USGS) classes [84].

4. Methodology

This study involved the following steps: (1) data acquisition and curation including topographic, hydrological, land use, and built-up areas, (2) hydraulic simulation and calibration, (3) cartographic processing. The overall flow chart is presented in Figure 3.

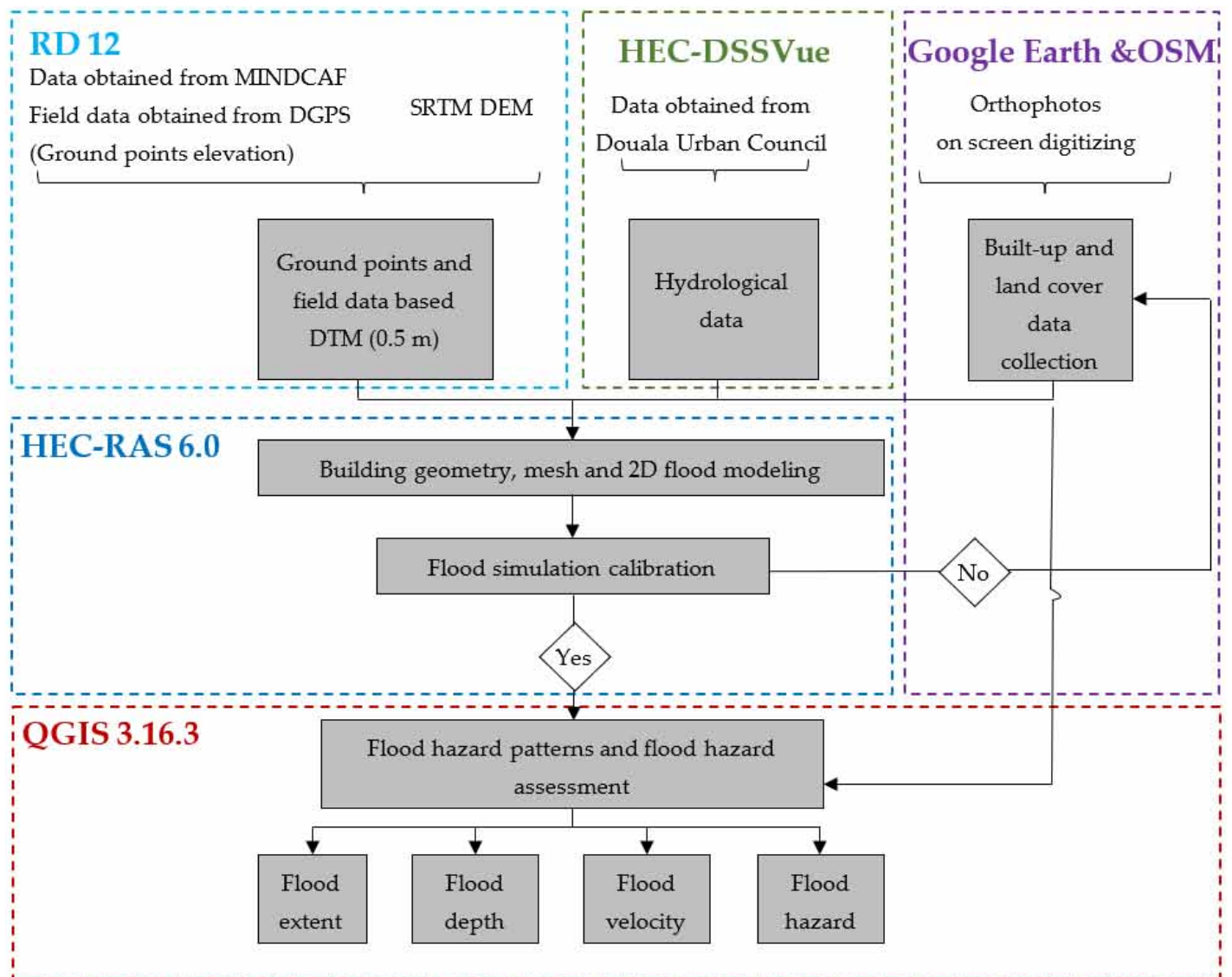


Figure 3. Overall methodology of the study.

4.1. HEC-RAS Modeling

The 2D HEC-RAS configuration solves either the Saint-Venant equation (Equation (1)) or the diffusion wave approximation (Equations (2) and (3)).

$$\frac{\partial \zeta}{\partial t} + \frac{\partial p}{\partial x} + \frac{\partial q}{\partial y} = 0 \quad (1)$$

$$\frac{\partial p}{\partial t} + \frac{\partial}{\partial x} \left(\frac{p^2}{h} \right) + \frac{\partial}{\partial y} \left(\frac{pq}{h} \right) = - \frac{n^2 pg \sqrt{p^2 + q^2}}{h^2} - gh \frac{\partial \zeta}{\partial x} + pf + \frac{\partial}{\rho \partial x} (h \tau_{xx}) + \frac{\partial}{\rho \partial y} (h \tau_{xy}) \quad (2)$$

$$\frac{\partial q}{\partial t} + \frac{\partial}{\partial y} \left(\frac{q^2}{h} \right) + \frac{\partial}{\partial x} \left(\frac{pq}{h} \right) = - \frac{n^2 qg \sqrt{p^2 + q^2}}{h^2} - gh \frac{\partial \zeta}{\partial y} + qf + \frac{\partial}{\rho \partial y} (h \tau_{yy}) + \frac{\partial}{\rho \partial x} (h \tau_{xy}) \quad (3)$$

where h is the water depth (m), p and q are the specific flow in the x and y directions ($\text{m}^2 \text{s}^{-1}$), respectively, ζ is the surface elevation (m), g is the acceleration due to gravity ($\text{m}^2 \text{s}^{-2}$), n is the Manning's Roughness coefficient ($\text{m}^{-1/3} \text{s}$), ρ is the water density (kg m^{-3}), τ_{xx} , τ_{yy} , and τ_{xy} are the component of effectiveness shear stress, and f is the Coriolis (s^{-1}). When diffusion wave mode is selected, the inertial terms of the momentum are neglected [59].

To ensure numerical stability of the model [55], the time step was defined according to the Courant–Friedrichs–Lewy condition [59,65] (Equation (4)).

$$C = \frac{V \Delta T}{\Delta x} \leq 1.0 \text{ (avec } C_{max} = 3.0) \text{ ou } \Delta T \leq \frac{\Delta x}{V} \text{ (avec } C = 1.0) \quad (4)$$

where C is the Courant number, V is the velocity (m s^{-1}), ΔT is the time step (s), and Δx is the grid cell size (m).

The model geometry was built in Rasmapper and HEC-RAS editor using the DTM to represent the ground surface. Manning's values associated with each zone were defined according to land use and land cover classes. Hydraulics structures were drawn following their characteristics measured during the survey. Rasmapper was used to build a computational mesh at 30×30 m spatial resolution on the entire study area. Mesh refinements were integrated into the initial grid in particular zones (banks, major roads, and bridges). The final mesh contained over 4067 cells comprising three to eight faces. Two internal boundary conditions were set to flow the hydrograph upstream the Ngongue and Kondi Rivers (at gauges G8 and G7, respectively). The tide acting at the outlet of the Tongo Bassa watershed situated 3.15 km downstream the modeled area was considered negligible because reverse flow was not observed during field survey. The external boundary condition was set to normal depth and the friction slope was estimated near the outlet of the simulation domain (at "Pont Cassé"). The computational mesh grid, the boundary conditions (internal and external), and the hydraulics structures built in the HEC-RAS model to simulate the 21st flood event in Makèpè Missokè are presented in Figure 4 below. The model was run between 21 August 2020 00:00 and 22 August 2020 08:00 with a computational interval of 5 s using HEC-RAS version 6.0.0, Windows 10 (64-bits), Intel® Core™ i7-6700HQ CPU 2.60 GHz, and 8 GB of DDR3 RAM. The Model outputs interval was set to 5 min for model performance and calibration. All other HEC-RAS unsteady computation options and tolerances were set to default.

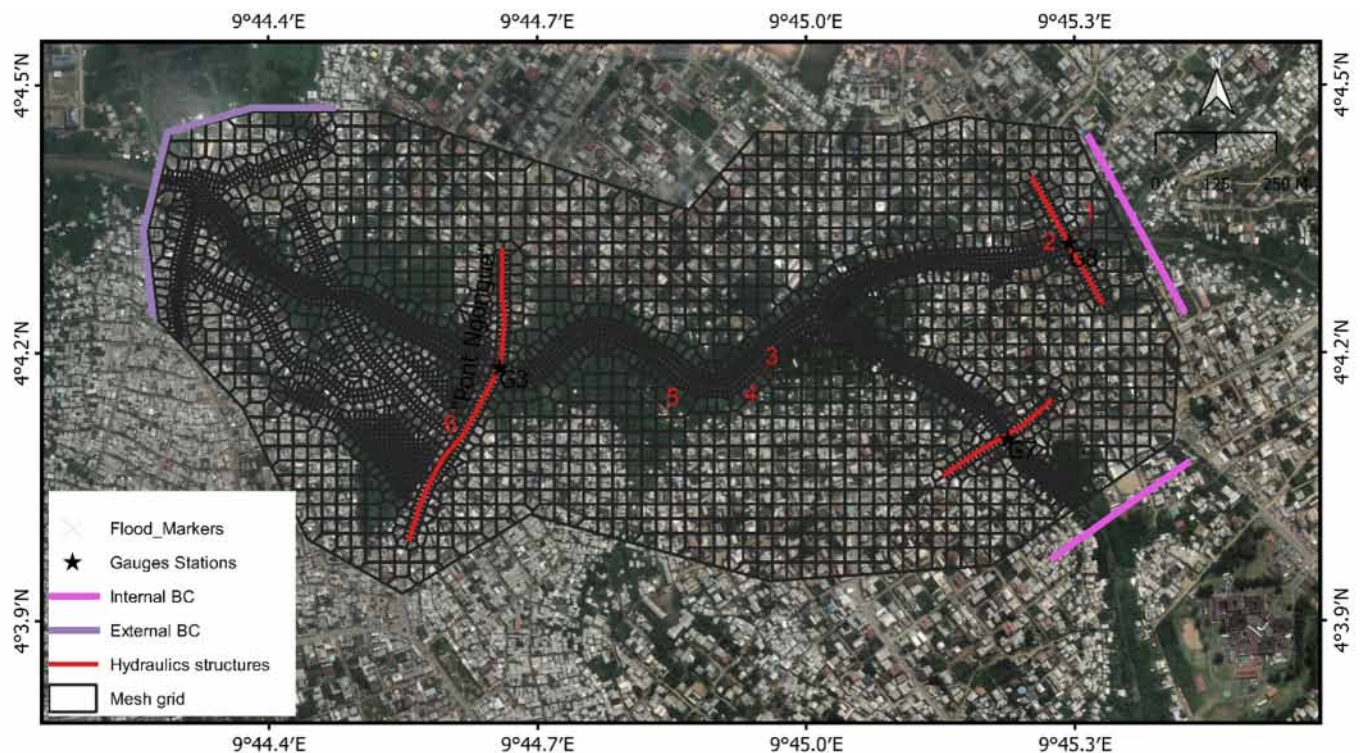


Figure 4. Simulation domain, computational mesh grid, and boundary conditions defined for assessing flood in Makèpè Missokè.

4.2. HEC-RAS Model Calibration

The HEC-RAS model was calibrated using the observed data collected at six gauging sites (flood marks), as presented on Figure 1D. The method consisted in adjusting the model parameters to accurately reproduce the water surface elevation observed on flood marks in the studied area [67]. To achieve this, the Manning’s Roughness coefficients were adjusted to obtain the desired accuracy. Model performance was assessed using statistical indices including [85,86]: the Nash–Sutcliffe efficiency (NSE), the relative deviation in the Nash–Sutcliffe efficiency (E_{rel}), and the root-mean-square error ($RMSE$) given by Equations (5)–(7).

$$NSE = 1 - \frac{\sum_{t=1}^T (O_i - P_i)^2}{\sum_{t=1}^T (O_i - \bar{O})^2} \quad (5)$$

$$E_{rel} = 1 - \frac{\sum_{i=1}^n \left(\frac{O_i - P_i}{O_i} \right)^2}{\sum_{i=1}^n \left(\frac{O_i - \bar{O}}{\bar{O}} \right)^2} \quad (6)$$

$$RMSE = \sqrt{\frac{\sum_{i=1}^n (P_i - O_i)^2}{N}} \quad (7)$$

where O_i = observed water levels, P_i = simulated water levels, \bar{O} = average observed water levels, \bar{P} = average simulated water levels, and N = total number of observations.

To date, no water marks were available to undertake validation of the model on another flood event. To overcome this data gap, the calibrated model was used to retrieve the water level at the water gauging station G3 (at “Pont Ngongue”) in the middle part of the simulation domain.

4.3. Flood Hazard Assessment

In this study, flood hazard classification was based on the Australian Institute for Disaster Resilience (AIDR, 2017) criteria [87]. This method was based on objective indicators such as flood depth, flow velocity, or a combination of these criteria [55,58,65,87]. According to this criterion, the hazard categories based on the vulnerability curves are as follows: H1 ($D \times V \leq 0.3 \text{ m}^2/\text{s}$), H2 ($0.3 \text{ m}^2/\text{s} < D \times V \leq 0.6 \text{ m}^2/\text{s}$), H3 ($0.6 \text{ m}^2/\text{s} < D \times V \leq 1.2 \text{ m}^2/\text{s}$), H4 ($1.2 \text{ m}^2/\text{s} < D \times V \leq 2 \text{ m}^2/\text{s}$), H5 ($2 \text{ m}^2/\text{s} < D \times V \leq 4 \text{ m}^2/\text{s}$), and H6 ($D \times V > 4 \text{ m}^2/\text{s}$). The hazard description based on the AIDR criterion is shown in Table 1.

Table 1. Hazard classification based on flood depth and flood velocity according to the AIDR [87].

Flood Hazard	$D \times V \text{ (m}^2/\text{s)}$	Hazard Description
H1	≤ 0.3	Generally safe for vehicles, people, and buildings
H2	≤ 0.6	Unsafe for small vehicles
H3	≤ 1.2	Unsafe for vehicles, children, and the elderly
H4	≤ 2	Unsafe for vehicles and people
H5	≤ 4	Unsafe for vehicles and people. All the building types are vulnerable to structural damage. Some less robust building types are vulnerable to failure.
H6	> 4	Unsafe for vehicles and people. All building types considered vulnerable to failure

5. Results

5.1. Calibration of the 2D HEC-RAS Model

The HEC-RAS model is calibrated by adjusting the simulated-to-observed water levels during peak flow discharge at six flood marks within the Makèpè Missokè neighborhood. The optimized Manning roughness values (n) for floodplain calibration are $n = 0.12$ and $n = 0.17$, respectively, for urban and vegetation areas. The residual difference ranges from 0.02 m to 0.44 m (Table 2). The most significant differences are observed at flood marks numbered #4 (0.19 m) and #6 (0.44 m). These differences can be explained by the high water marks measurement and the DTM used as input in the hydraulic model. The highest water marks present uncertainties related to building materials, flood time durations, and local flow conditions. Building materials and flood time durations induce capillary rises that deal with inaccuracies in the measurement (during marking and surveying with DGPS). The local flow condition due to the presence of buildings can influence locally the water surface elevation. Furthermore, flood mark numbered #6 is located near an artificial lake created by sand extraction activity. The bathymetry of this lake is poorly represented in DTM, which results in a weak representation of the flood retention effect in this area.

Table 2. Comparison of the water levels (meters) between those observed and simulated by HEC-RAS at six different points located in Makèpè Missokè floodplain during the 21 August 2020 flood.

Calibration	Water Levels (m) Flood 2020		Difference = S – O
N°	(O) Observed	(S) Simulated	
1	8.64	8.84	0.2
2	7.51	7.54	0.03
3	6.82	6.8	−0.02
4	6.56	6.75	0.19
5	6.65	6.62	−0.03
6	5.78	6.22	0.44
	NSE		0.94
	Erel		0.92
	RMSE		0.21

The observed and HEC-RAS simulated stage associated with the 21st August 2020 at gauge G3 (“Pont Ngongue”) in Makèpè Missokè are presented in Figure 5. The results showed that the model was unable to retrieve accurately the water levels recorded at gauging station G3. The simulated maximum water level overestimated those observed by 80 cm. This difference was consistent with the one observed for the water mark numbered #6 (overestimated by 44 cm). The imperfections in the DTM may be associated with the poor representation of the lake located downstream at the G3 gauge station. A more representative DTM that better reflects the terrain configuration would allow better results to be obtained. However, the flood dynamics was well captured by the model during the flood and the recession phases. It can be inferred that the developed model based on available data was fairly consistent with observations during the event.

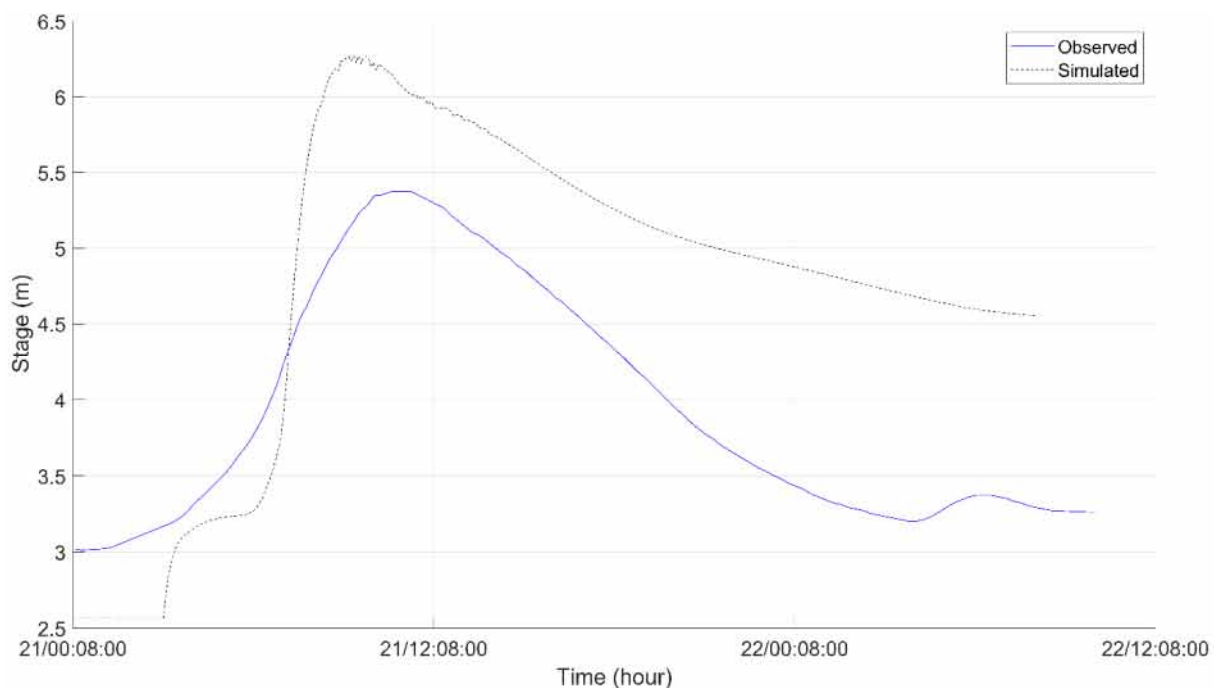


Figure 5. Comparison of the observed and HEC-RAS simulated stage that occurred on the 21 August 2020 at gauge G3 (“Pont Ngongue”) in Makèpè Missokè.

5.2. Flood Extent and Flood Depth

The simulated flood extent based on the computed dry cells covered an area of about 81.84 ha. The entire width of the major river channel was inundated. The flood depth map was generated by considering the maximum recorded depth in each cell of the flooded zone. The maximum flood depth recorded for the simulation was 4.48 m in the main channel of the Ngongue River (Figure 6). About 2210 buildings were impacted by this flood event with 31% (683 buildings) affected by a flood depth lower than 0.25 m, about 26% (587 buildings) between 0.25 m and 0.5 m, 39% (871 buildings) by a flood depth between 0.5 m and 1 m, and finally 3% (69 buildings) exposed to a flood depth between 1 m and 2 m. Flood depths higher than 2 m were observed in the main river channel and concerned only hydraulics structures and not buildings. Undersized hydraulics structures were inundated (more than 1.2 m over the deck/roadway) and resulted in the unavailability of the road crossing the river.

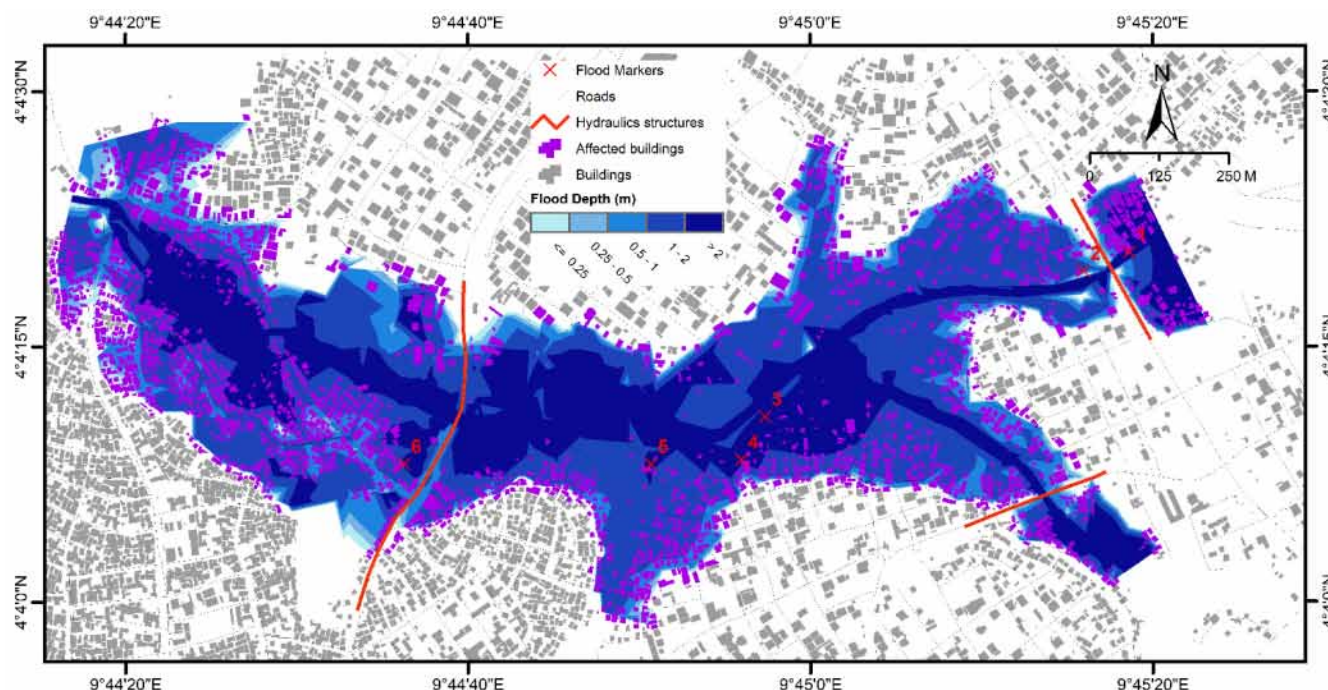


Figure 6. Flood depth (m) within the “Makèpè Missokè” floodplain for the August 2020 (model output).

5.3. Flood Velocity

The flood velocity map was obtained by calculating the maximum velocity in each cell recorded over the simulation period (21 August 2020 00:00 to 22 August 2020 08:00). The maximum modeled flood velocity was 10.15 m/s at an average velocity in the modeled area of 0.5 m/s. These velocities were classified into five categories (Figure 7): very low ($V \leq 0.25$ m/s), low ($0.25 < V \leq 0.5$ m/s), medium ($0.5 < V \leq 0.75$ m/s), high ($0.75 < V \leq 1$ m/s), and very high ($V > 1$ m/s). A percentage of 65% (1441 buildings) were affected by velocities that did not exceed 0.25 m/s, 23% (500 buildings) by flood velocities between 0.25 and 0.5 m/s, 7% (165 buildings) by velocities between 0.5 and 0.75 m/s, 3% (69 buildings) between 0.75 and 1 m/s, and finally less than 2% (35 buildings) were affected by velocities above 0.5 m/s. In this zone characterized by weak variations in the topography and a dense vegetation in the main channel, these velocities presented a good agreement with the ground reality. The model showed important velocities ($V > 1$ m/s) close to hydraulics structures (bridges at “Vallée Hôpital Général”, “Vallée La Conquête”, and “Pont Cassé”), indicating considerable flow constriction by the bridges and thus ultimately an increased risk of failure. Furthermore, during the high water, the flow obstruction generated backwater and significant retention, resulting in flooding in the upstream part of the bridges. This finding is particularly relevant close to the bridges in the study area (G3, G7, G8), where we observed a submergence that interrupted roads during the floods. In the downstream part of the studied area, at “Pont Cassé”, the pinching of the flow was mainly due to topography. A high flow velocity has been observed here previously: indeed, it caused the collapse of a previous bridge after an historical flood, which gave it the evocative name of “Pont Cassé”, i.e., broken bridge.

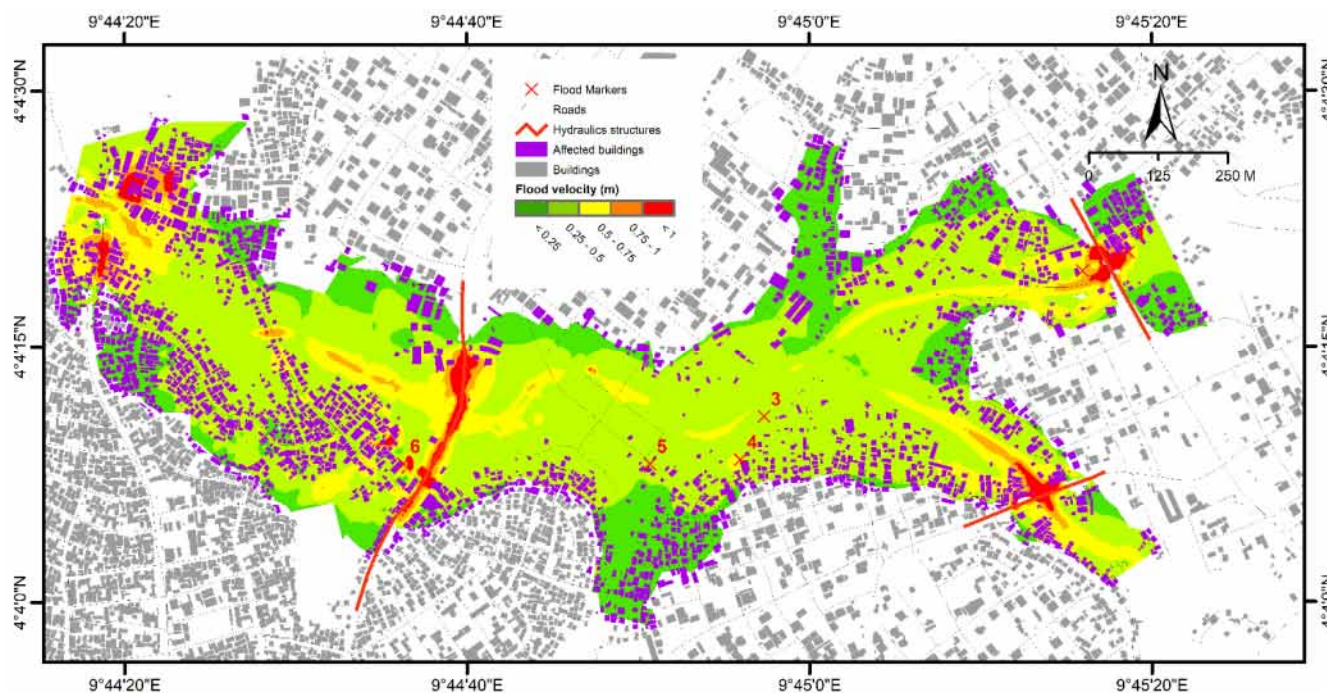


Figure 7. Flood velocity (m/s) within the “Makèpè Missokè” floodplain for the August 2020.

5.4. Flood Arrival Times and Duration

The flood arrival map in hours was generated in the flooded area from the start time of the simulation (on 21 August 2020 00:00) and for a depth threshold of 0.5 m. Arrival times in the study area varied between 4 h and 9 h. The map presented in Figure 8A revealed two main zones in the modeled area limited by the “Pont Ngongue” (at water level gauge G3): the first upper bridge that was flooded under at least 0.5 m of water depth after seven hours (6.5 h), and the second lower bridge flooded after at least eight hours (8.5 h). This finding is particularly relevant close to the hydraulics structures in the study area and confirms the significant retention resulting in flooding the upper bridges. On the other hand, a higher flood depth (1.5 m and 2.5 m respectively) occurred after 9 h and revealed the fast mobilization of the floodplain for the evacuation of this flood.

The flood duration map for the 2020 flood event in Makèpè Missokè was generated in the same way as the flood arrival times. For the 0.5 m threshold, the duration of submergence in the modelled area reached up to 30 h in the main river channels and varied between 6 h and 16 h in the floodplain (Figure 8B). Three hotspot areas flooded for more than 24 h, i.e., around the confluence of the Ngongue and Kondi rivers, the areas upstream of the Ngongue Bridge, and the “Pont Cassé”. We note that the duration of flooding in this area was less than one day. This result contrasts the testimonies of the residents who declared to have been flooded during several days. The influence of tide at the outlet of the Tongo Bassa watershed is likely the reason for the underestimation of flood depth and flood duration times in the study area.

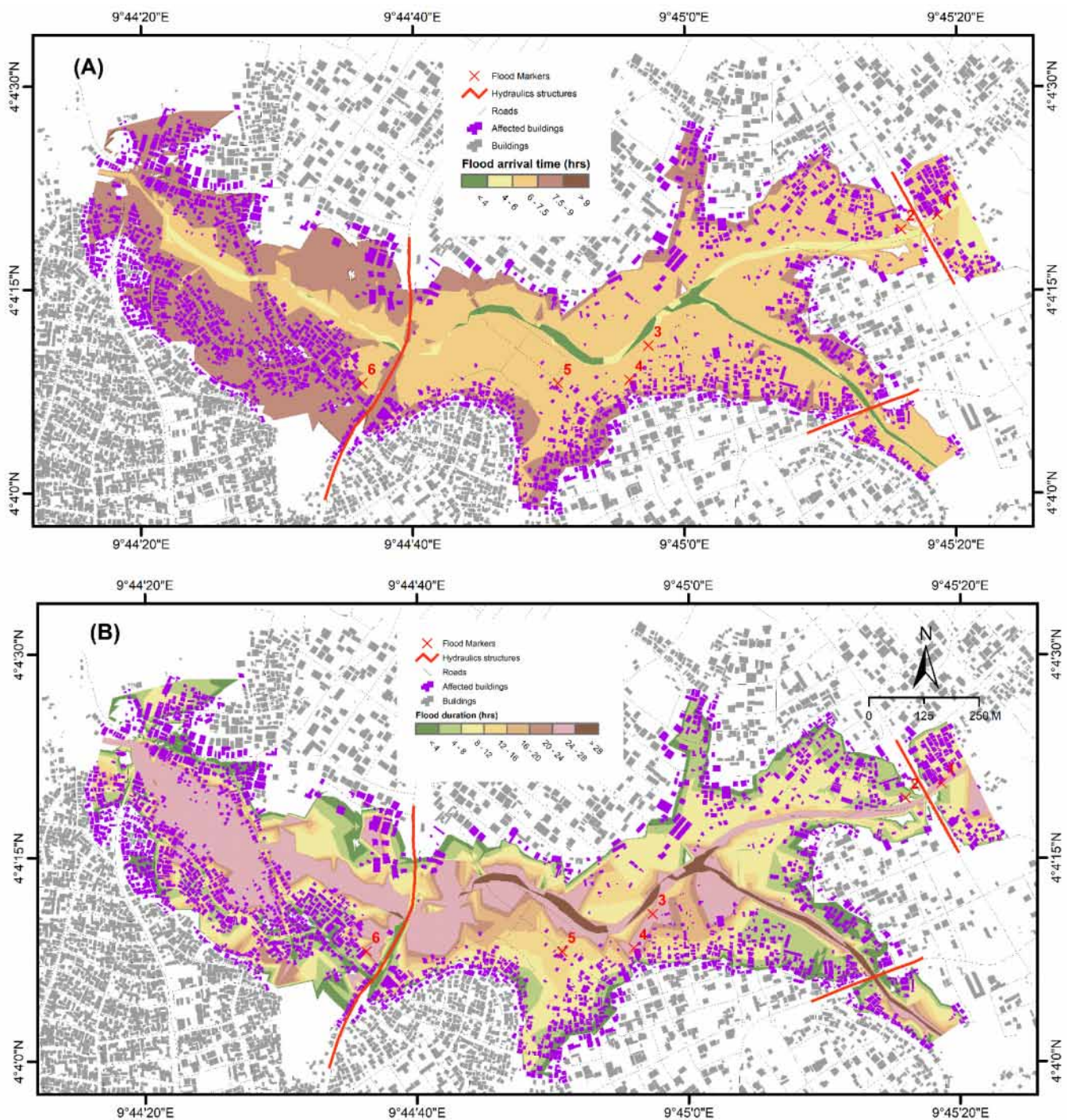


Figure 8. (A) Flood arrival. (B) Flood duration for 0.5 m threshold.

5.5. Flood Hazard Assessment

The AIDR criterion [87] is used to classify exposure from low to high hazards (See Figure 9). Combining the modeled flow velocity and inundation level, 54% (1196 buildings) are located in classes H1 and H2, nearly 44% (966 buildings) in class H3, less than 2% (35 buildings) in class H4, and only 0.4% and 0.2% (9 and 4 buildings), respectively, are located in classes H5 and H6. This analysis shows that the flood hazard in the Makèpè Missokè district globally varies between H1 and H3. According to AIDR, this presents little risk for constructions in concrete. However, many constructions made of temporary materials such as cardboard, wood, or metal sheets are present in the low-lying areas affected by regular flooding, presenting considerable risks for the fast-growing population

in these zones. Further, in the widespread H2/H3 zones, mobility is significantly affected for people and vehicles, in particular, for children, the elderly, or those with reduced mobility. In the minor riverbed, the hazard varies from H4 to H6, i.e., the exposure to a higher risk for the people having set-up constructions there, or directly on the banks of the watercourse.

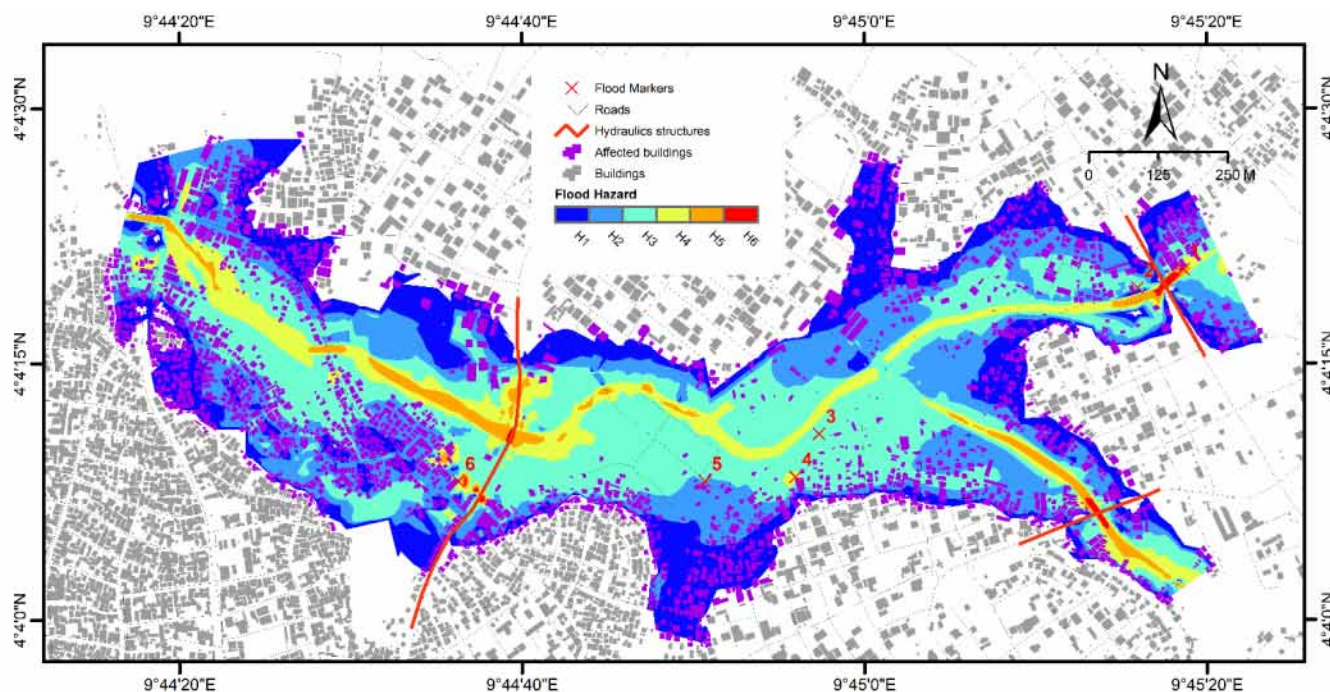


Figure 9. Flood hazard classification according to the AIDR criteria [87].

The number of people affected can be estimated by taking into consideration either the population density estimated from 25 to 380 inhabitants [72], or the average household size estimated at 5.6 inhabitants [34] in the study area. Based on these two assertions, the number of affected persons ranges between 2050 and 31,160 when comparing the population density and 12,376 when taking into account the household size.

The hydraulic structures are exposed to significant risks (H6). The reduction in the section of flow at the structures involves a rise in the surface of water and a significant increase in flow velocity. In addition, the significant water depth and flow velocities at the vicinity of the hydraulics structures results in significant mobility difficulties because of the submergence of these major transport axes, thus also affecting economic activity as well as potential disaster relief mobilization.

6. Discussions

The model provides important spatially resolved information on the major flood recorded by the recently installed Tongo Bassa watershed environmental observatory, on 21st August 2020 in the Makèpè Missokè neighborhood. Based on available topographic data, the model developed showed a good agreement between the observed and simulated water surface elevation at the peak flow discharges ($NSE = 0.94$, $Erel = 0.92$, $RMSE = 0.21$ m).

The present study of a flood event in the Makèpè Missokè neighborhood complements previous analyses [19,25], where the floodplain delineation criteria were based on hydrogeomorphological and historical analyses, without detailed hydrological flow modeling. In addition to the delineation of the extent of the flooded area based on hydrological parameters, this study provides significantly improved insights particularly on the dynamics of propagation of the flood wave.

Moreover, the simulated velocity in the main channel indicates a potential sediment transport and deposition that could gradually obstruct the hydraulic structures. Moreover,

the simulated velocity confirms the [72] statement concerning that the rivers in the Tongo Bassa watershed would be in an erosive phase in the upstream part and in an accreting phase downstream.

The mapping of flood arrival times provides important new information on the time needed to set-up a flood warning system or the time needed for an emergency intervention. In turn, the mapping of flood duration provides important information on the time required for a return to normalcy in the disaster area after a major flood. This information is highly relevant to decision makers and managers to efficiently deploy emergency resources to be engaged in case of a major flood event.

The hazard classification over the model domain is conducted by combining the flood depth and the flood velocity maps using the AIDR method [87], resulting in spatially resolved maps of risk to which the residents are exposed in the Makèpè Missokè district. The information provided by this study contrasts with a previous study [25] regarding the evaluation of potentially wet areas by calculating the Beven–Kirby index (1975) computed in GIS software using some physical catchment characteristics.

The model developed in this study proposed detailed information on the flood hazard associated with the 21 August 2020 flood. In order to improve the accuracy and utility of the model and its application to flood hazard management, the return period of the rainfall event that causes this flood needs to be determined. A translation of this major event in terms of the return period using frequency analysis would allow the decision-makers to have a better appreciation of the risk against which to protect and to establish a more relevant delimitation of the zones at risk with a view to developing and implementing coherent strategies to reduce the impact of floods.

7. Conclusions

This study was carried out to characterize the hazard associated with the major flood event that took place in August 2021 in the Makèpè Missokè district in the city of Douala using 2D HEC-RAS modeling. The model was calibrated using high water marks in six points at peak flow discharge and the observed stage recorded at gauge G3 situated in the middle part of the simulation domain. The results showed that the flood dynamic is well captured and the 2D hydraulic model was able to retrieve the observed water surface elevation ($NSE = 0.94$, $E_{rel} = 0.92$, $RMSE = 0.21$ m). The August 2020 event used the major riverbed for evacuation of the flood with depth and velocity that represent a real hazard risk for the households. The low-lying hydrological center of the investigated area was classified between H3 and H5; thus, it may be unsafe for vehicles, children, the elderly, or buildings, and in some cases can cause structural damage and failure of less robust buildings. Significant velocities were recorded near the hydraulics structures. The floodplain remained underwater for several hours after the end of the event. Conversely, some sites were covered by no more than 0.5 m of water depth for more than a day. The developed 2D HEC-RAS model is satisfactory considering the available data.

The methodology developed and the results are also and, above all, useful for the local administration, especially the DUC, which intervenes at different levels and scales in the management of floods in the city of Douala. The results can be helpful for the design of the planned bridges and the implementation of a more effective maintenance or the protection strategy of the existing ones particularly sensitive to high velocities. The knowledge of flood extent, depth, and hazard classification allows the municipality to design structural mitigation measures and equipment (drains, flood control basin, etc.) and to prohibit constructions in the more dangerous areas or to subject them to specific structural requirements, all things contributing to the move toward a proactive flood management policy.

Author Contributions: Conceptualization, J.Y.-A.I., A.C.-D. and R.O.; methodology, J.Y.-A.I., A.C.-D., S.B., W.E.S., R.O. and T.S.; software, J.Y.-A.I. and A.C.-D.; validation, J.Y.-A.I., A.C.-D. and S.B.; formal analysis, J.Y.-A.I. and A.C.-D.; investigation, J.Y.-A.I., A.C.-D., S.B., W.E.S. and R.O.; data analyses, J.Y.-A.I., A.C.-D., W.E.S., J.-P.B. and T.S.; writing—original draft preparation, J.Y.-A.I.; writing—review

and editing, J.Y.-A.I., A.C.-D., S.B., W.E.S., R.O., R.N., J.-C.N., J.M.O.O., F.D.K. and J.E.; visualization, J.Y.-A.I., A.C.-D., S.B., W.E.S. and R.O.; supervision, R.N., J.-C.N., J.M.O.O., F.D.K., J.E. and T.S.; project administration, R.O., J.M.O.O. and J.-J.B.; funding acquisition, R.O. and J.-J.B. All authors have read and agreed to the published version of the manuscript.

Funding: This work was carried out with the scientific, technical, and financial support of the Interdisciplinary Research Program on Climate and Urban Environment (PRInCE), within the framework of the AFD Convention CCM 1362.01K of the project “Douala, Sustainable City: Sustainable development and valorization of the Makèpè Missokè site”, co-funded by the French Global Environment Facility (FGEF), the French Development Agency (FDA), and the Douala City Council (DCC). The PRInCE was conducted under the scientific auspices of the French Research Institute for Sustainable Development (IRD) and the Laboratory of Technology and Applied Science, University Institute of Technology of the University of Douala. However, the DCC, FGEF, and the FDA do not intend to give any approval or disapproval to the opinions expressed in this paper; these must be considered as specific to the authors. Additional funding for equipment (DGPS) was provided by the ANR @RAction chair of excellence medLOC (ANR-14-ACHN-0007-01—T. Stieglitz).

Data Availability Statement: Data used in this study were collected with the institutional support of the DUC which ensures their archiving and distribution. These data are not available online. However, they are available on request from the DUC.

Acknowledgments: The authors want to thank Patherson Vanique Donfack Necdem, the one responsible for the environmental observatory installed on the Tongo Bassa river basin, for data acquisition and survey. The authors want to thank Loic Biblos Douhonang Tedongmo for topographic data acquisition.

Conflicts of Interest: The authors declare no conflict of interest.

References

1. Mann, M.E.; Emanuel, K.A. Atlantic Hurricane Trends Linked to Climate Change. *Eos Trans. Am. Geophys. Union* **2006**, *87*, 233. [CrossRef]
2. Knutson, T.R.; McBride, J.L.; Chan, J.; Emanuel, K.; Holland, G.; Landsea, C.; Held, I.; Kossin, J.P.; Srivastava, A.K.; Sugi, M. Tropical Cyclones and Climate Change. *Nat. Geosci.* **2010**, *3*, 157–163. [CrossRef]
3. Diaconu, D.C.; Costache, R.; Popa, M.C. An Overview of Flood Risk Analysis Methods. *Water* **2021**, *13*, 474. [CrossRef]
4. Nematchoua, M.K.; Orosa, J.A.; Reiter, S. Climate Change: Variabilities, Vulnerabilities and Adaptation Analysis—A Case of Seven Cities Located in Seven Countries of Central Africa. *Urban Clim.* **2019**, *29*, 100486. [CrossRef]
5. Saha, F.; Nkemta, D.T.; Tchindjang, M.; Voundi, É.; Fendoung, P.M. Production des risques dits «naturels» dans les grands centres urbains du Cameroun. *Nat. Sci. Soc.* **2018**, *26*, 418–433. [CrossRef]
6. Tchindjang, M.; Fendoung, P.M. Une Afrique Atlantique avec des Villes sous L’eau! Construire des Villes Côtières Sans Inondations? 2019, p. 30. Available online: <http://hdl.handle.net/2268/238401> (accessed on 12 July 2021).
7. Vedeld, T.; Kombe, W.J.; Kweka-Msale, C.; Ndour, N.M.; Coly, A.; Hellevik, S. Multi-Level Governance, Resilience to Flood Risks and Coproduction in Urban Africa. In *Urban Vulnerability and Climate Change in Africa: A Multidisciplinary Approach*; Pauleit, S., Coly, A., Fohlmeister, S., Gasparini, P., Jørgensen, G., Kabisch, S., Kombe, W.J., Lindley, S., Simonis, I., Yeshitela, K., Eds.; Future City; Springer International Publishing: Cham, Switzerland, 2015; pp. 287–318. ISBN 978-3-319-03982-4.
8. Wambo, E.M.N. Hygiène Du Cadre de Vie et Action Communautaire à Nylon-Douala. In *Visages et Défis des Principales Villes Camerounaises*; Université de Montréal: Montréal, QB, Canada, 2008; Volume 7, ISBN 978-2-921903-01-1.
9. Fonteh, M.; Esteves, L.S.; Gehrels, W.R. Mapping and Valuation of Ecosystems and Economic Activities along the Coast of Cameroon: Implications of Future Sea Level Rise. *Coastline Rep. EUCC Int. Approaches Coast. Res. Theory Pract.* **2009**, *13*, 47–63.
10. Nji Fogwe, Z. Mitigating and Managing Regional Geo-Environmental Hazards within a Decentralisation Transition in Cameroon. *J. Hum. Ecol.* **2010**, *30*, 187–195. [CrossRef]
11. Bang, H.N. General Overview of the Disaster Management Framework in Cameroon. *Disasters* **2014**, *38*, 562–586. [CrossRef]
12. Munji, C.A.; Bele, M.Y.; Nkwatoh, A.F.; Idinoba, M.E.; Somorin, O.A.; Sonwa, D.J. Vulnerability to Coastal Flooding and Response Strategies: The Case of Settlements in Cameroon Mangrove Forests. *Environ. Dev.* **2013**, *5*, 54–72. [CrossRef]
13. Meva’a Abomo, D.; Fouda, M.; Siméon Nguehan, B.; Ebana, A.A.; Pola, G.M. Vulnérabilité de l’agriculture urbaine aux inondations dans le bassin versant du Mbanya à Douala (Cameroun). *Ann. Rech. Urb.* **2015**, *110*, 164–173. [CrossRef]
14. Ndongo, B.; Mbouendeu, S.L.; Tirmou, A.A.; Njila, R.N.; Dalle, J.D.M. Tendances pluviométriques et impact de la marée sur le drainage en zone d’estuaire: Cas du Wouri au Cameroun. *Afr. Sci. Rev. Int. Sci. Technol.* **2015**, *11*, 173–182. [CrossRef]
15. Yengoh, G.T.; Fogwe, Z.N.; Armah, F.A. Floods in the Douala Metropolis, Cameroon: Attribution to Changes in Rainfall Characteristics or Planning Failures? *J. Environ. Plan. Manag.* **2017**, *60*, 204–230. [CrossRef]
16. Tanessong, R.S.; Vondou, D.A.; Djomou, Z.Y.; Igri, P.M. WRF High Resolution Simulation of an Extreme Rainfall Event over Douala (Cameroon): A Case Study. *Model. Earth Syst. Environ.* **2017**, *3*, 927–942. [CrossRef]

17. CUD (2012)—Plan Directeur d'Urbanisme de Douala à l'horizon 2025. Édité. République du Cameroun/Communauté Urbaine de Douala. 239 pages. Available online: http://www.cldocs.bianguenetworks.info/cudxmedia2014/PDU_Plan%20Horizon%2025.pdf (accessed on 12 July 2021).
18. Ministère de l'Administration Territoriale et de la Décentralisation (MINATD). Plan National de Contingence du Cameroun, 2011. Available online: https://plateformecholera.info/attachments/article/450/Cameroune_%20Plan_%20contingence_2011.pdf (accessed on 12 July 2021).
19. Bruckmann, L.; Amanejieu, A.; Moffo, M.O.Z.; Ozer, P. Analyse géohistorique de l'évolution spatio-temporelle du risque d'inondation et de sa gestion dans la zone urbaine de Douala (Cameroun). *Physio-Géo Géogr. Phys. Environ.* **2019**, *XIII*, 91–113. [\[CrossRef\]](#)
20. Tchiadeu, G.; Olinga, O.J.M. La ville de Douala: Entre baisse des précipitations et hausse des températures. In *Les Climats Régionaux: Observation et Modélisation, 25ème Colloque de l'Association Internationale de Climatologie (Grenoble)*; Bigot, S., Rome, S., Eds.; Université Joseph Fourier: Grenoble, France, 2012; pp. 727–732.
21. Assako, R.J.A.; Nsegbe, A.; Bley, D. Proposition d'un Modèle de Restructuration d'un Front d'urbanisation Anarchique: Le Cas de Song-Mahop, Un Quartier Périphérique de Douala (Cameroun). *Gabonica* **2008**, *2*, 5–22.
22. Bang, H.N. Governance of Disaster Risk Reduction in Cameroon: The Need to Empower Local Government. *Jambá J. Disaster Risk Stud.* **2013**, *5*, 10. [\[CrossRef\]](#)
23. Ngoran, S.D.; Xue, X. Addressing Urban Sprawl in Douala, Cameroon: Lessons from Xiamen Integrated Coastal Management. *J. Urban Manag.* **2015**, *4*, 53–72. [\[CrossRef\]](#)
24. Mbaha, J.P.; Tchounga, G.B. Caractérisation de l'urbanisation dans les zones littorales des pays tropicaux: Exemple du Wouri. *Espace Géogr. Soc. Maroc.* **2020**, *33–34*, 215–226. [\[CrossRef\]](#)
25. Zogning, M.M.O.; Tonye, E.; Ambara, G.; Tsalefack, M. Cartography of flood prone areas and assessment of flooding housing in Douala (Cameroon). In Proceedings of the United Nations International Conference on Space-based Technologies for Disaster Management—"Disaster risk identification, assessment and monitoring", Beijing, China, 7–9 November 2012; Available online: <https://www.researchgate.net/publication/273321869> (accessed on 12 July 2021).
26. Metzger, A.; David, F.; Valette, P.; Rode, S.; Martin, B.; Desarthe, J.; Linton, J. Entretenir la mémoire des inondations via les repères de crue? *Dév. Durable Territ. Économie Géogr. Polit. Droit Sociol.* **2018**, *9*, 28. [\[CrossRef\]](#)
27. Coeur, D.; Lang, M. L'information Historique Des Inondations: L'histoire Ne Donne-t-Elle Que Des Leçons? *Houille Blanche* **2000**, *2*, 79–84. [\[CrossRef\]](#)
28. Is New Orleans Safer Today Than When Katrina Hit 10 Years Ago?—Scientific American. Available online: <https://www.scientificamerican.com/article/is-new-orleans-safer-today-than-when-katrina-hit-10-years-ago/> (accessed on 12 July 2021).
29. Tsalefac, M.; Ngoufo, R.; Nkwambi, W.; Tatsangue, E.D.; Fobissie, B.L. Fréquences et quantités des précipitations journalières sur le territoire camerounais. *Publ. AIC* **2003**, *15*, 359–367.
30. Ndille, R.; Belle, J.A. Managing the Limbe Floods: Considerations for Disaster Risk Reduction in Cameroon. *Int. J. Disaster Risk Sci.* **2014**, *5*, 147–156. [\[CrossRef\]](#)
31. Fogwe, Z.N.; Tchotsoua, M. Evaluation géographique de deux décennies de lutte contre les inondations dans la ville de Douala (Cameroun). In Proceedings of the Actes des Journées Scientifiques Inter-réseaux de l'Agence Universitaire de la Francophonie (JSI-RAUF), Hanoï, Vietnam, 6–9 November 2007; pp. 6–9.
32. Mbaha, J.P.; Olinga, J.M.; Tchiadeu, G. Cinquante ans de conquête spatiale à Douala: D'héritage colonial en construction à patrimoine socio-spatial vulnérable aux risques naturels. In *Actes du Colloque du Cinquantenaire de la Réunification du Cameroun*; 2013; pp. 13–14. Available online: <https://catalog.ihsn.org/index.php/citations/77657> (accessed on 12 July 2021).
33. Bang, H.; Miles, L.; Gordon, R. Evaluating Local Vulnerability and Organizational Resilience to Frequent Flooding in Africa: The Case of Northern Cameroon. *foresight* **2019**, *21*, 266–284. [\[CrossRef\]](#)
34. Napi Wouapi, H. *Framework for Municipal Adaptation Plan Case Study of Douala V Municipality Missokè Site, a Floods Hot Spot in Douala V Municipality*; Konrad-Adenauer-Stiftung, Yaoundé, Cameroon. December 2018.
35. Meva a Abomo, D.; Fouda, M.; Bonglam Chofor, Z.; Kamwo, M. Analyse Spatiale Du Risque d'Inondation Dans Le Bassin Versant Du Mbanya à Douala, Capitale Économique Du Cameroun. In Proceedings of the Novatech 2010—7ème Conférence internationale sur les techniques et stratégies durables pour la gestion des eaux urbaines par temps de pluie/7th International Conference on sustainable techniques and strategies for urban water management, Lyon, France, 27 June–1 July 2010; pp. 1–10.
36. Munji, C.A.; Bele, M.Y.; Idinoba, M.E.; Sonwa, D.J. Floods and Mangrove Forests, Friends or Foes? Perceptions of Relationships and Risks in Cameroon Coastal Mangroves. *Estuar. Coast. Shelf Sci.* **2014**, *140*, 67–75. [\[CrossRef\]](#)
37. Nguh, B.S.; Anumveh, N.N. Endemic Hydro Climatic Flood Hazards in Some Cameroon Coastal Cities: The Hand of Man or the Work of Nature? *Mod. Concepts Dev. Agron.* **2018**, *2*, 155–165. [\[CrossRef\]](#)
38. Fute, E.; Steve, T. Analysis and Implementation of a Platform for Natural Disaster Management: Case of Flood in Douala Town. Master's Thesis, University of Buea, Buea, Cameroon, 2019. [\[CrossRef\]](#)
39. Nojang, E.N.; Jensen, J. Conceptualizing Individual and Household Disaster Preparedness: The Perspective from Cameroon. *Int. J. Disaster Risk Sci.* **2020**, *11*, 333–346. [\[CrossRef\]](#)
40. Niba, M.L.F.; Gideon, S. Evaluation of the Impacts of Sea Level Rise Hazards in Douala-Cameroon. *OALib* **2021**, *8*, e7427. [\[CrossRef\]](#)

41. Bladé, E.; Cea, L.; Corestein, G.; Escolano, E.; Puertas, J.; Vázquez-Cendón, E.; Dolz, J.; Coll, A. Iber: Herramienta de simulación numérica del flujo en ríos. *Rev. Int. Metod. Numér. Cálculo Diseño Ing.* **2014**, *30*, 1–10. [\[CrossRef\]](#)
42. Manfreda, S.; Samela, C.; Gioia, A.; Consoli, G.G.; Iacobellis, V.; Giuzio, L.; Cantisani, A.; Sole, A. Flood-Prone Areas Assessment Using Linear Binary Classifiers Based on Flood Maps Obtained from 1D and 2D Hydraulic Models. *Nat. Hazards* **2015**, *79*, 735–754. [\[CrossRef\]](#)
43. Dasallas, L.; Kim, Y.; An, H. Case Study of HEC-RAS 1D–2D Coupling Simulation: 2002 Baeksan Flood Event in Korea. *Water* **2019**, *11*, 2048. [\[CrossRef\]](#)
44. Chomba, I.C.; Banda, K.E.; Winsemius, H.C.; Chomba, M.J.; Mataa, M.; Ngwenya, V.; Sichingabula, H.M.; Nyambe, I.A.; Ellender, B. A Review of Coupled Hydrologic-Hydraulic Models for Floodplain Assessments in Africa: Opportunities and Challenges for Floodplain Wetland Management. *Hydrology* **2021**, *8*, 44. [\[CrossRef\]](#)
45. Nkwunonwo, U.C.; Whitworth, M.; Baily, B. A Review of the Current Status of Flood Modelling for Urban Flood Risk Management in the Developing Countries. *Sci. Afr.* **2020**, *7*, e00269. [\[CrossRef\]](#)
46. Fernández, A.; Najafi, M.R.; Durand, M.; Mark, B.G.; Moritz, M.; Jung, H.C.; Neal, J.; Shastry, A.; Laborde, S.; Phang, S.C.; et al. Testing the Skill of Numerical Hydraulic Modeling to Simulate Spatiotemporal Flooding Patterns in the Logone Floodplain, Cameroon. *J. Hydrol.* **2016**, *539*, 265–280. [\[CrossRef\]](#)
47. Dimitriadis, P.; Tegos, A.; Oikonomou, A.; Pagana, V.; Koukouvinos, A.; Mamassis, N.; Koutsoyiannis, D.; Efstratiadis, A. Comparative Evaluation of 1D and Quasi-2D Hydraulic Models Based on Benchmark and Real-World Applications for Uncertainty Assessment in Flood Mapping. *J. Hydrol.* **2016**, *534*, 478–492. [\[CrossRef\]](#)
48. Zhang, Y.; Wang, Y.; Zhang, Y.; Luan, Q.; Liu, H. Multi-Scenario Flash Flood Hazard Assessment Based on Rainfall–Runoff Modeling and Flood Inundation Modeling: A Case Study. *Nat. Hazards* **2021**, *105*, 967–981. [\[CrossRef\]](#)
49. Jamali, B.; Bach, P.M.; Deletic, A. Rainwater Harvesting for Urban Flood Management—An Integrated Modelling Framework. *Water Res.* **2020**, *171*, 115372. [\[CrossRef\]](#)
50. Knebl, M.R.; Yang, Z.-L.; Hutchison, K.; Maidment, D.R. Regional Scale Flood Modeling Using NEXRAD Rainfall, GIS, and HEC-HMS/RAS: A Case Study for the San Antonio River Basin Summer 2002 Storm Event. *J. Environ. Manag.* **2005**, *75*, 325–336. [\[CrossRef\]](#)
51. Patel, D.P.; Ramirez, J.A.; Srivastava, P.K.; Bray, M.; Han, D. Assessment of Flood Inundation Mapping of Surat City by Coupled 1D/2D Hydrodynamic Modeling: A Case Application of the New HEC-RAS 5. *Nat. Hazards* **2017**, *89*, 93–130. [\[CrossRef\]](#)
52. Ben Khalfallah, C.; Saidi, S. Spatiotemporal Floodplain Mapping and Prediction Using HEC-RAS—GIS Tools: Case of the Mejerda River, Tunisia. *J. Afr. Earth Sci.* **2018**, *142*, 44–51. [\[CrossRef\]](#)
53. Rangari, V.A.; Sridhar, V.; Umamahesh, N.V.; Patel, A.K. Floodplain Mapping and Management of Urban Catchment Using HEC-RAS: A Case Study of Hyderabad City. *J. Inst. Eng. India Ser. A* **2019**, *100*, 49–63. [\[CrossRef\]](#)
54. Chen, Y.-H.; Mossa, J.; Singh, K.K. Floodplain Response to Varied Flows in a Large Coastal Plain River. *Geomorphology* **2020**, *354*, 107035. [\[CrossRef\]](#)
55. Mihiu-Pintilie, A.; Cîmpianu, C.I.; Stoleriu, C.C.; Pérez, M.N.; Paveluc, L.E. Using High-Density LiDAR Data and 2D Streamflow Hydraulic Modeling to Improve Urban Flood Hazard Maps: A HEC-RAS Multi-Scenario Approach. *Water* **2019**, *11*, 1832. [\[CrossRef\]](#)
56. Arseni, M.; Rosu, A.; Calmuc, M.; Calmuc, V.A.; Iticescu, C.; Georgescu, L.P. Development of Flood Risk and Hazard Maps for the Lower Course of the Siret River, Romania. *Sustainability* **2020**, *12*, 6588. [\[CrossRef\]](#)
57. Mai, D.T.; De Smedt, F. A Combined Hydrological and Hydraulic Model for Flood Prediction in Vietnam Applied to the Huong River Basin as a Test Case Study. *Water* **2017**, *9*, 879. [\[CrossRef\]](#)
58. Huțanu, E.; Mihiu-Pintilie, A.; Urzica, A.; Paveluc, L.E.; Stoleriu, C.C.; Grozavu, A. Using 1D HEC-RAS Modeling and LiDAR Data to Improve Flood Hazard Maps Accuracy: A Case Study from Jijia Floodplain (NE Romania). *Water* **2020**, *12*, 1624. [\[CrossRef\]](#)
59. Quirogaa, V.M.; Kurea, S.; Udoa, K.; Manoa, A. Application of 2D Numerical Simulation for the Analysis of the February 2014 Bolivian Amazonia Flood: Application of the New HEC-RAS Version 5. *Ribagua* **2016**, *3*, 25–33. [\[CrossRef\]](#)
60. Zeiger, S.J.; Hubbard, J.A. Measuring and Modeling Event-Based Environmental Flows: An Assessment of HEC-RAS 2D Rain-on-Grid Simulations. *J. Environ. Manag.* **2021**, *285*, 112125. [\[CrossRef\]](#)
61. Baldassarre, G.D.; Montanari, A. Uncertainty in River Discharge Observations: A Quantitative Analysis. *Hydrol. Earth Syst. Sci.* **2009**, *13*, 913–921. [\[CrossRef\]](#)
62. Reistad, S.K.; Petersen-Overleir, A.; Bogetveit, L.J. Setting up Rating Curves Using HEC-RAS. *J. Korea Water Resour. Assoc.* **2007**, *3*, 20–30.
63. Spada, E.; Sinagra, M.; Tucciarelli, T.; Biondi, D. Unsteady State Water Level Analysis for Discharge Hydrograph Estimation in Rivers with Torrential Regime: The Case Study of the February 2016 Flood Event in the Crati River, South Italy. *Water* **2017**, *9*, 288. [\[CrossRef\]](#)
64. Iroume, J.Y.-A.; Sone Essoh, W.; Onguéné, R.; Colmet-Daage, A.; Stieglitz, T.; Bogning, S.; et Braun, J.-J. Réalisation d'un Modèle hydraulique et hydrologique calibré et validé sur l'ensemble du bassin versant du Tongo Bassa, Douala-Cameroun. 2021; Unpublish report.
65. Urzică, A.; Mihiu-Pintilie, A.; Stoleriu, C.C.; Cîmpianu, C.I.; Huțanu, E.; Pricop, C.I.; Grozavu, A. Using 2D HEC-RAS Modeling and Embankment Dam Break Scenario for Assessing the Flood Control Capacity of a Multi-Reservoir System (NE Romania). *Water* **2021**, *13*, 57. [\[CrossRef\]](#)

66. Psomiadis, E.; Tomanis, L.; Kavvadias, A.; Soulis, K.X.; Charizopoulos, N.; Michas, S. Potential Dam Breach Analysis and Flood Wave Risk Assessment Using HEC-RAS and Remote Sensing Data: A Multicriteria Approach. *Water* **2021**, *13*, 364. [CrossRef]
67. Naeem, B.; Azmat, M.; Tao, H.; Ahmad, S.; Khattak, M.; Haider, S.; Ahmad, S.; Khoro, Z.; Goodell, C. Flood Hazard Assessment for the Tori Levee Breach of the Indus River Basin, Pakistan. *Water* **2021**, *13*, 604. [CrossRef]
68. Zelenáková, M.; Fijko, R.; Labant, S.; Weiss, E.; Markovič, G.; Weiss, R. Flood Risk Modelling of the Slatvinec Stream in Kružlov Village, Slovakia. *J. Clean. Prod.* **2019**, *212*, 109–118. [CrossRef]
69. Yalcin, E. Assessing the Impact of Topography and Land Cover Data Resolutions on Two-Dimensional HEC-RAS Hydrodynamic Model Simulations for Urban Flood Hazard Analysis. *Nat. Hazards* **2020**, *101*, 995–1017. [CrossRef]
70. Dysarz, T.; Szalkiewicz, E.; Wicher-Dysarz, J. Long-Term Impact of Sediment Deposition and Erosion on Water Surface Profiles in the Ner River. *Water* **2017**, *9*, 168. [CrossRef]
71. Tarar, Z.R.; Ahmad, S.R.; Ahmad, I.; Hasson, S.; Khan, Z.M.; Washakh, R.M.A.; Ateeq-Ur-Rehman, S.; Bui, M.D. Effect of Sediment Load Boundary Conditions in Predicting Sediment Delta of Tarbela Reservoir in Pakistan. *Water* **2019**, *11*, 1716. [CrossRef]
72. Boum-Nkot, S.N.; Ketchemen-Tandia, B.; Ndje, Y.; Envouttou, H.; Ebonji, C.R.; Huneau, F. Origin of Mineralization of Groundwater in the Tongo Bassa Watershed (Douala-Cameroon). *Res. J. Environ. Earth Sci.* **2015**, *7*, 29–41. [CrossRef]
73. Onguene, R.; Pemha, E.; Lyard, F.; Du-Penhoat, Y.; Nkoue, G.; Duhaut, T.; Njeugna, E.; Marsaleix, P.; Mbiaka, R.; Jombe, S.; et al. Overview of Tide Characteristics in Cameroon Coastal Areas Using Recent Observations. *Open J. Mar. Sci.* **2014**, *5*, 81–98. [CrossRef]
74. Din, N.; Ngo-Massou, V.M.; Essomè-Koum, G.L.; Ndema-Nsombo, E.; Kottè-Mapoko, E.; Nyamsi-Moussian, L. Impact of Urbanization on the Evolution of Mangrove Ecosystems in the Wouri River Estuary (Douala Cameroon). In *Coastal Wetlands: Alteration and Remediation*; Finkl, C.W., Makowski, C., Eds.; Coastal Research Library; Springer International Publishing: Cham, Switzerland, 2017; Volume 21, pp. 81–131. ISBN 978-3-319-56178-3.
75. Djuikom, E.; Temgoua, E.; Jugnia, L.; Nola, M.; Baane, M. Pollution Bactériologique Des Puits d’eau Utilisés Par Les Populations Dans La Communauté Urbaine de Douala—Cameroun. *Int. J. Biol. Chem. Sci.* **2009**, *3*, 967–978. [CrossRef]
76. Njueya, A.; Likeng, J.; Nono, A. Hydrodynamique et qualité des eaux souterraines dans le bassin sédimentaire de Douala (Cameroun): Cas des aquifères sur formations Quaternaires et Tertiaires. *Int. J. Biol. Chem. Sci.* **2012**, *6*, 1874–1894. [CrossRef]
77. Akoachere, J.-F.T.K.; Mbuntcha, C.K.P. Water Sources as Reservoirs of *Vibrio Cholerae*O1 and Non-O1 Strains in Bepanda, Douala (Cameroon): Relationship between Isolation and Physico-Chemical Factors. *BMC Infect. Dis.* **2014**, *14*, 421. [CrossRef] [PubMed]
78. Ketchemen-Tandia, B.; Boum-Nkot, S.N.; Ebonji, S.R.; Nlend, B.Y.; Envoutou, H.; Nzegue, O. Factors Influencing the Shallow Groundwater Quality in Four Districts with Different Characteristics in Urban Area (Douala, Cameroon). *J. Geosci. Environ. Prot.* **2017**, *5*, 99–120. [CrossRef]
79. Ndo, C.; Menze-Djantio, B.; Antonio-Nkondjio, C. Awareness, Attitudes and Prevention of Malaria in the Cities of Douala and Yaoundé (Cameroon). *Parasit. Vectors* **2011**, *4*, 181. [CrossRef]
80. Farr, T.G.; Rosen, P.A.; Caro, E.; Crippen, R.; Duren, R.; Hensley, S.; Kobrick, M.; Paller, M.; Rodriguez, E.; Roth, L.; et al. The Shuttle Radar Topography Mission. *Rev. Geophys.* **2007**, *45*. [CrossRef]
81. Yan, K.; Di Baldassarre, G.; Solomatine, D.P. Exploring the Potential of SRTM Topographic Data for Flood Inundation Modelling under Uncertainty. *J. Hydroinform.* **2013**, *15*, 849–861. [CrossRef]
82. Pangali Sharma, T.P.; Zhang, J.; Khanal, N.R.; Prodhan, F.A.; Nanzad, L.; Zhang, D.; Nepal, P. A Geomorphic Approach for Identifying Flash Flood Potential Areas in the East Rapti River Basin of Nepal. *IJGI* **2021**, *10*, 247. [CrossRef]
83. Nasiri, V.; Deljouei, A.; Moradi, F.; Sadeghi, S.M.M.; Borz, S.A. Land Use and Land Cover Mapping Using Sentinel-2, Landsat-8 Satellite Images, and Google Earth Engine: A Comparison of Two Composition Methods. *Remote Sens.* **2022**, *14*, 1977. [CrossRef]
84. Arcement, G.J.; Schneider, V.R. *Guide for Selecting Manning’s Roughness Coefficients for Natural Channels and Flood Plains*; Water Supply Paper; U.S. G.P.O.; For sale by the Books and Open-File Reports Section; U.S. Geological Survey: Denver, CO, USA, 1989; Volume 2339. [CrossRef]
85. Chow, V.T. *Open-Channel Hydraulics*; McGraw-Hill: New York, NY, USA, 1959; ISBN 978-0-07-085906-7.
86. Legates, D.; McCabe, G. Evaluating the Use of “Goodness-of-fit” Measures in Hydrologic and Hydroclimatic Model Validation. *Water Resour. Res.* **1999**, *35*, 233–241. [CrossRef]
87. AIDR (Australian Institute for Disaster Resilience). Australian Disaster Resilience Handbook 7 Managing the Floodplain: A Guide to Best Practice in Flood Risk Management in Australia (AIDR 2017). Available online: <https://www.preventionweb.net/publications/view/55084> (accessed on 12 July 2021).